Comparison of Urban Environment Factors for Solar-Powered Vehicles

Jiyoon Ku [1], Hyeong-Dong Park [2, 3]

[1] Dept. of Energy Systems Engineering, Seoul National University, 08826 Seoul, South Korea - rnldbs9808@snu.ac.kr
[2] Dept. of Energy Resources Engineering, Seoul National University, 08826 Seoul, South Korea - hpark@snu.ac.kr
[3] Research Institute of Energy and Resources, Seoul National University, 08826 Seoul, South Korea - hpark@snu.ac.kr

Keywords: Solar-powered Vehicle (SPV), Shadow analysis, Urban Shadow, Geographic Information Systems (GIS), Hillshade, Clean transportation

Abstract

Urban areas face significant environmental challenges, including high CO_2 emissions largely attributed to the transportation sector. Introducing solar-powered vehicles (SPVs) presents a promising solution to reduce urban carbon footprints. However, in dense urban settings, the effectiveness of SPVs is often compromised by shading from buildings, which significantly diminishes solar power generation. This study explores the impact of shading on urban roads, aiming to identify roads with substantial shadow variations that affect solar energy harvesting. Using Geographic Information Systems (GIS) and hillshade analysis, the study examines how nearby buildings and road orientation influence shadow variability. The findings reveal considerable variability in shadow throughout the year, with significant fluctuations during transitional months like February, August, October, and November. These results highlight the importance of considering shadow patterns in urban planning and vehicle routing to optimise the use of solar energy in urban settings.

1. Introduction

Air pollution from transportation in urban areas presents a significant challenge, exacerbated by the dense configuration of cityscapes which impedes the dispersal of contaminants (Rossi et al., 2020). Worldwide efforts are being made to decrease greenhouse gas emissions. The International Energy Agency reports that the transportation sector is responsible for 23% of global CO_2 emissions, with road transport contributing 74% of that total (IEA, 2023). Introducing electric vehicles (EVs), which use clean energy, in urban areas can significantly reduce urban carbon footprint (Bieker, 2021).

However, a recent issue has been the sensitivity of EV batteries to temperature, leading to battery failures (Senol et al., 2023). This problem is compounded by the limited number of designated charging stations, causing significant congestion when these stations are needed the most (Fan et al., 2023). In this context, Solar-powered vehicles (SPVs), or Vehicle-Integrated Photovoltaics (VIPVs) which can generate power even while driving, could be the long-term solution to such pressing urban issue.

In cities like Seoul, where parking spaces are scarce and charging while parked is not always feasible, waiting times at charging stations can be excessively long. Nevertheless, SPVs can serve as a valuable supplementary power source. By generating power during transit, they can utilise this auxiliary power effectively. However, commercial viability is hindered by their inefficiency. The effectiveness of these vehicles is heavily dependent on the urban environment—specifically, shading from surrounding buildings can significantly reduce their solar energy generation capabilities (Yoo, 2011).

This study explores the impact of shading from buildings in urban environments on the solar energy generation capabilities of SPVs. Specifically, it investigates how shadows cast onto urban roads which can reduce the power output of solar panels installed on vehicles. The analysis will focus on identifying which urban roads experience significant shadow variations throughout the day, potentially affecting solar energy harnessing.

Regarding vehicles, previous studies have utilised Geographic Information Systems (GIS) technology to predict photovoltaic (PV) power generation by considering factors like the vehicle's location, surrounding terrain, buildings, and the sun's movement. For instance, Oh et al. (2020) analysed the shadows reaching buses, and Kim et al. (2022) studied shadows on trains, utilising terrain information for solar power generation calculations. However, these studies only considered the predefined routes of buses and trains. Chalkias et al. (2013) created a Digital Terrain Model (DTM) and used GIS to calculate shadows but did not conduct detailed analyses for each spatiotemporal case of road shadows in urban settings.

Therefore, our research builds on these foundations by employing a Digital Surface Model (DSM) that includes terrain and building heights to study how shadows affect urban roads over time. We analyse the variations in shadow at one-hour intervals throughout the year, utilising the positions derived from splitting the roads at regular intervals as input values.

Understanding these shadow dynamics is crucial, as it directly influences the efficiency and practicality of SPVs in densely built areas. By mapping and modelling these variations, the research aims to contribute to the optimisation of urban planning and vehicle routing to enhance solar energy utilisation. This approach not only aids in maximising the potential of solar-powered transportation but also supports broader environmental goals by optimising renewable energy usage in urban settings.

2. Study area

The study focuses on Seoul, the capital city of South Korea, characterised by its dense urban architecture and heavy traffic. Seoul features a total of 707,292 buildings and approximately 10,260 km of roadways (MOLIT, 2021; NGII, 2023). This diversity in building heights and densities creates significant variations in shadow patterns across the roads. In parts of the city, like shown in Figure 1.b, large buildings cast long shadows over these roads, and as depicted in Figure 1.c, the varied orientation of Seoul's roads alongside the surrounding buildings significantly influences these shadow effects.

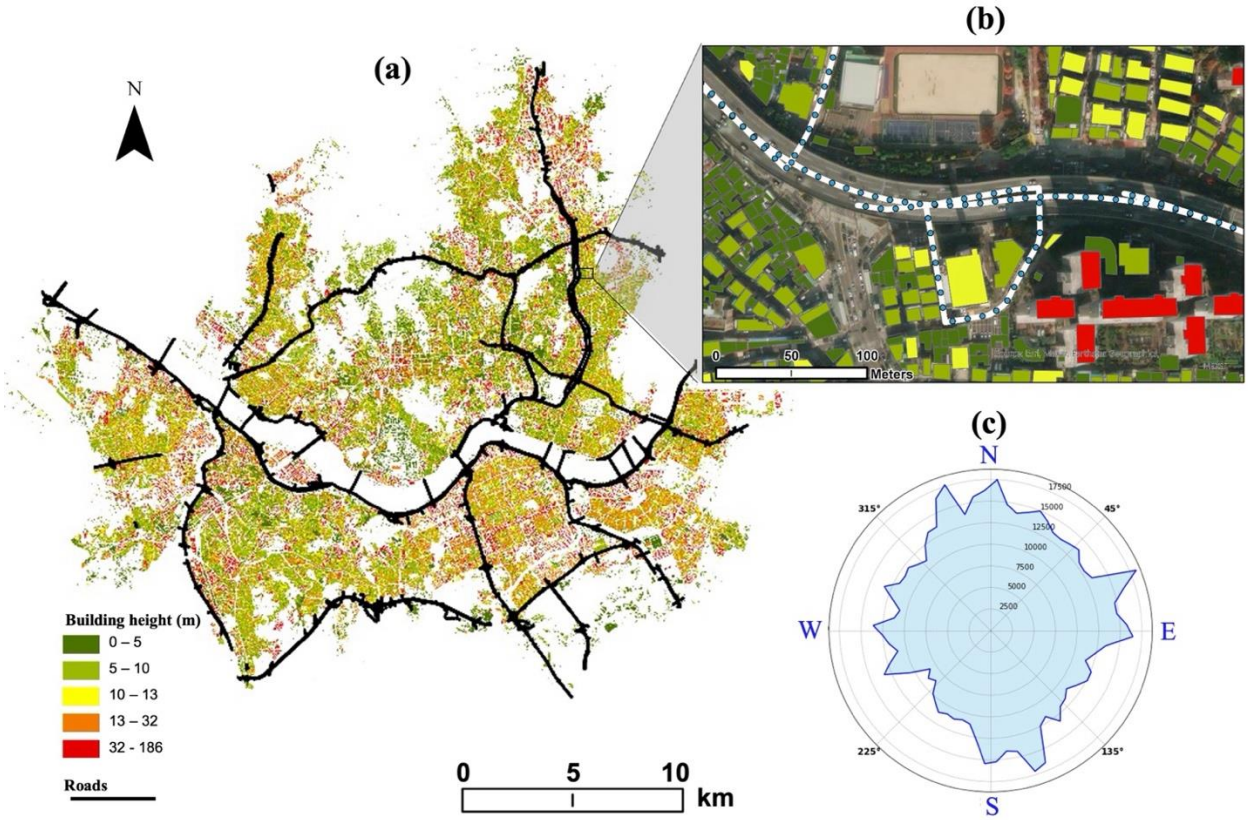

Figure 1. Study area: (a) Building heights and major roads with high traffic,
(b) Zoomed-in view with measurement points along the road, (c) Distribution of road azimuths.

3. Methods

In this study, the analysis of shadows on roads was conducted using through three main phases: (i) A DSM was created to include the elevation of both natural and man-made features to analyse shading effects. (ii) The top 25% of the busiest roads in Seoul over 2022 and 2023 were selected, and measurement points were set at 10 m intervals along these roads, totalling 50,849 points. (iii) The hillshade tool was used to determine shadow occurrence hourly throughout the year when the sun's elevation was above 0 degrees, categorising the results into fully shaded or not shaded. Lastly, daily standard deviations were calculated to assess shadow variability, grouping the roads by vertices into 2,072 segments for detailed analysis.

3.1 Digital Surface Model construction

The DSM was constructed to precisely capture the urban landscape of Seoul. For this analysis, ArcGIS Pro, a leading GIS analysis software, was utilised. DSM integrates detailed data on building heights. Building data, including the number of floors and area were sourced from the Ministry of Land, Infrastructure and Transport (MOLIT, 2021). Each building's height was calculated by multiplying the number of floors by an average floor height of 2.7 m. These data were then combined with DEM from the ASTER GDEM, which provides a base elevation at a 30 m spatial resolution (METI and NASA, 2023). The resolution was further refined to 3 m to enhance the accuracy of shadow modelling.

3.2 Extracting Measuring Points

For this analysis, top 25% of roads by traffic volume over the recent years 2022 and 2023 were selected (TOPIS, 2023). Having 520 km length in total (NGII, 2023). Measurement points were strategically placed at 10 m intervals along these roads to ensure comprehensive coverage and detailed data collection. This approach allowed for a granular analysis of shadow impacts across different times of the day and varying traffic conditions.

3.3 Shading analysis

3.3.1 Hillshade algorithm: Hillshade, used for illustrating shaded relief from a DSM, requires the altitude and azimuth of the light source for computation (Esri, 2023). By modelling shadows, it is possible to determine which cells are shaded at any given time via equation 1. Cells in shadow are marked with a value of 0, while those not shaded are marked from 1 to 255. For simplicity, values greater than 1 are reclassified to 1, creating a binary output. For instance, if the sun's elevation angle is bigger than the angle between a building and a measurement point, the area is non-shaded (value 1); otherwise, it is shaded (value 0) as illustrated in Figure 2.

$$Hillshade = 255 \times \{[\cos(Z) \times \cos(S)] + [\sin(Z) \times \sin(S) \times \cos(\gamma - A)]\} \quad (1)$$

where Z = Solar zenith angle (radian)
S = Surface slope angle (radian)
γ = Solar azimuth angle (radian)
A = Surface aspect angle (radian)

3.3.2 Shadow Variability on urban roads: Shadow data, captured using the hillshade method, was collected hourly only during sunlight hours over the year. By 2023, this totaled 4,421 hours. To understand shadow variability, the standard deviation of shadow intensity was computed from data points along Seoul's major roads, which were recorded every 10 m, totaling 50,849 points. These points were grouped by road vertices into 2,072 road segments, to calculate daily standard deviations. This analysis providing insights into how often and how significantly vehicles might be impacted by reduced solar exposure by shading.

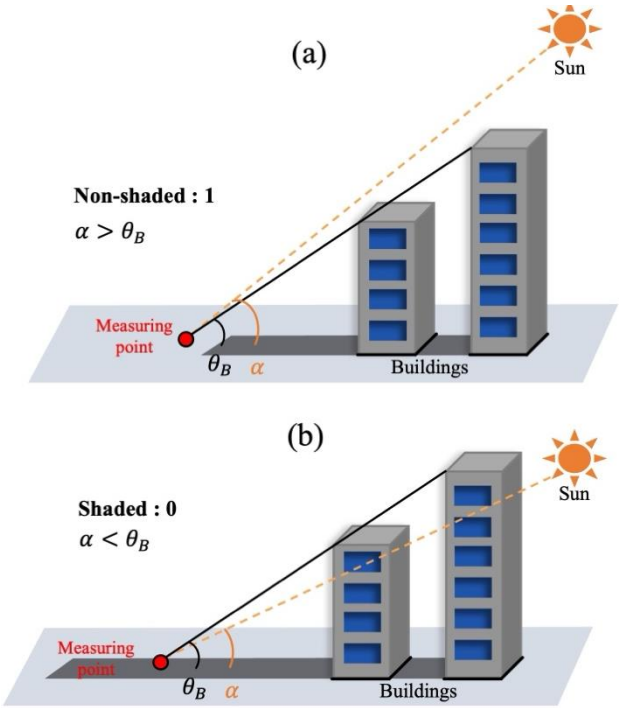

Figure 2. Illustration of building shadows due to the relative difference between the sun's altitude angle (α) and the angle from buildings to the measuring point (θ_B): (a) Measuring point non-shaded ($\alpha > \theta_B$), (b) Measuring point shaded ($\alpha < \theta_B$).

4. Results

4.1 Standard deviation throughout the year

To assess the year-round impact of shadows, this study analysed the variability of shadows on urban roads using standard deviation, and shadow intensity using mean values. Table 1 presents a statistical summary of daily shadow values, showcasing standard deviations and means by month. The table also includes statistical observations such as the minimum, first quartile (Q1), median, and third quartile (Q3) to provide a comprehensive view of the data.

The standard deviation, representing the variability in daily shadow, indicated notable differences across the months. Higher standard deviations were observed in February, April, August, October, suggesting a greater variability in shadow intensities during these months. This higher variability aligns with seasonal transitions where the sun’s angle changes significantly, affecting the length and intensity of shadows cast by urban structures.

Across all months, the minimum standard deviation values consistently registered at zero, indicating complete consistency of shadows. This consistency points to predictable periods each day, likely around solar noon, when shadows are minimal due to the sun's high position. Alternatively, when shadows are continuously present, the standard deviation can still be 0. However, as shown in Table 1, the distribution of the average shadow values indicates that the Q1 of the mean is higher than 0.9 (1 indicating no shadows). Therefore, when the standard deviation is 0, it likely corresponds to a period without shadows.

The analysis of shadow variability throughout the year indicates a clear seasonal pattern. During the summer months of May, June, and July, the Q1 results of standard deviation were near zero, suggesting consistent shadow values conducive to optimal solar energy harvesting. In contrast, during the transitional months of February, August, October, and November, the standard deviation values were significantly higher. This increase reflects a greater variability in shadow presence, influenced by the sun’s lower elevation, which results in more pronounced fluctuations in shadows throughout the day.

Figure 3 clearly delineate the seasonal variations in shadow intensity, with summer months showing lower variability, conducive to solar energy use. Transition months exhibited higher variability and intensity, posing challenges for consistent solar power generation. These findings are crucial for urban planning and the deployment of SPVs, highlighting the need to consider seasonal and monthly shadow patterns to optimise the placement and operation of solar energy systems in urban environments.

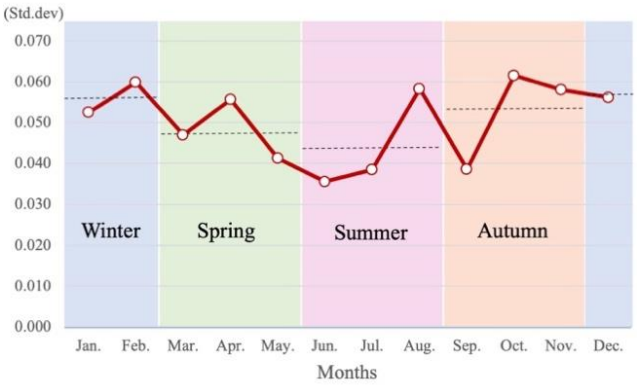

Figure 3. Monthly and seasonal variations of daily shadow standard deviations.

The results were stratified using a heatmap that categorised annual standard deviations and averages, divided into ten class quantiles (Figure 4). The heatmap reveals a distinct inverse relationship between the average shadow presence and its variability. In this study, shadow values were calculated such that a value of 0 indicates fully shaded conditions, whereas a value of 1 represents no shade. Smaller average shadow values imply a significant presence of shadows, corresponding to clusters near 1 on the mean axis. These areas typically lie close to the 10th quantile on the standard deviation axis, indicating high shadow variability. Conversely, when there are fewer shadows, as indicated by mean clusters close to 10, there is low shadow serial variability. This pattern highlights the impact of shadow presence on variability, illustrating that broader shadow coverage tends to accompany higher fluctuations in shadow length.

Stats	Jan.	Feb.	Mar.	Apr.	May.	Jun.	Jul.	Aug.	Sep.	Oct.	Nov.	Dec.

Std. Dev	**Mean**	0.053	0.060	0.047	0.056	0.041	0.036	0.038	0.058	0.039	0.062	0.058	0.056
	Min	0.000	0.000	0.000	0.000	0.000	0.000	0.000	0.000	0.000	0.000	0.000	0.000
	Q1	0.013	0.022	0.012	0.024	0.000	0.000	0.000	0.023	0.003	0.026	0.020	0.012
	Med	0.047	0.054	0.041	0.050	0.034	0.027	0.030	0.052	0.031	0.056	0.052	0.052
	Q3	0.075	0.081	0.066	0.074	0.060	0.052	0.056	0.078	0.056	0.082	0.079	0.080
	Max	0.484	0.484	0.492	0.484	0.474	0.469	0.476	0.480	0.495	0.503	0.490	0.497
Mean	**Mean**	0.960	0.957	0.971	0.976	0.982	0.985	0.983	0.976	0.978	0.960	0.953	0.948
	Min	0.000	0.318	0.508	0.679	0.702	0.714	0.696	0.687	0.566	0.489	0.000	0.000
	Q1	0.946	0.947	0.963	0.968	0.975	0.978	0.976	0.967	0.972	0.951	0.941	0.931
	Med	0.974	0.975	0.983	0.982	0.988	0.991	0.989	0.981	0.988	0.976	0.973	0.967
	Q3	0.994	0.992	0.996	0.993	1.000	1.000	1.000	0.994	0.999	0.991	0.993	0.992
	Max	1.000	1.000	1.000	1.000	1.000	1.000	1.000	1.000	1.000	1.000	1.000	1.000

Table 1. Monthly statistical overview of daily shadow metrics: standard deviation and mean intensity

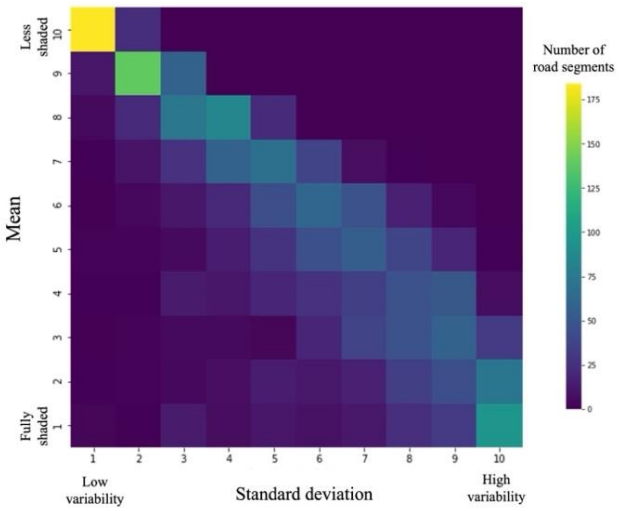

Figure 4. Heatmap of relationships between daily shadow mean and standard deviation, grouped into deciles.

4.2 GIS results spatially overviewed

4.2.1 Urban shadow dynamics -spatial variability: To explore urban shadow dynamics spatially, Figure 5.a shows the ArcGIS Pro-generated annual average of daily standard deviation, presented with a five-class quantile legend evenly distributing data values across each class. In this classification, section b exhibits low shadow variability, whereas section c displays high shadow variability. The impact of shadow variability is further examined in Figures 5.b and c, focusing on October—identified previously as having the highest variability. For presentation, October 15th was designated, and observations taken at three-hour intervals starting from 8 AM

Figure 5.b shows a road with low shadow presence and low shadow variability. On this road section, shadows were observed only in the early morning (8 AM) due to one tall building. For the other time of the day, there were no shadows since the distance between the road and buildings was wide, and the buildings were low, resulting in shorter shadows. Additionally, in October late afternoon (5 PM), when the sun is at a low angle, shadows appear horizontally. Given that this section of the road also runs horizontally, it is less affected by shadows.

Figure 5.c depicts road sections where shadows were prevalent at low sun altitudes (8 AM and 5 PM), resulting in longer shadows and consequently higher variability. In contrast to Figure 5.b, the distance between the road and buildings in this area is narrower, and the buildings are relatively taller, leading to a greater impact from shadows. Moreover, shadows extend horizontally in the morning and evening, and since the road runs vertically, it is more affected by these shadows.

4.2.2: Influence of road direction: The study also explores how road direction affects shadow variability. It analysed the shadow patterns of 2,072 roads, which were categorised into eight distinct directions: North-South (NS), Northeast/Southwest (NE/SW), East-West (EW), and Southeast/Northwest (SE/NW). Monthly patterns are displayed in Figure 6.

From April to August, roads oriented in the NS and NE/SW directions exhibited higher shadow variability compared to other road orientations. Despite this period generally having lower shadow intensity and variability on average, the NS and particularly the NE/SW oriented roads experienced more frequent changes in shadow presence due to the buildings on right and left side. This suggests that buildings block the sunlight more effectively when the sun is positioned in the east or west, rather than directly south.

During the winter months of October, November, and December, roads oriented in the EW and SE/NW directions had higher shadow variability than other orientations. This period is characterised by generally stronger shadow intensity and higher variability. During these months, buildings obstruct the sunlight when it is in the south, leading to greater variability of shadows cast on the roads.

This comprehensive analysis of shadow variability not only provides insights into the daily and seasonal dynamics of urban shadows but also emphasises the critical influence of built environment configurations, such as building proximity and road orientation, on shadow behavior.

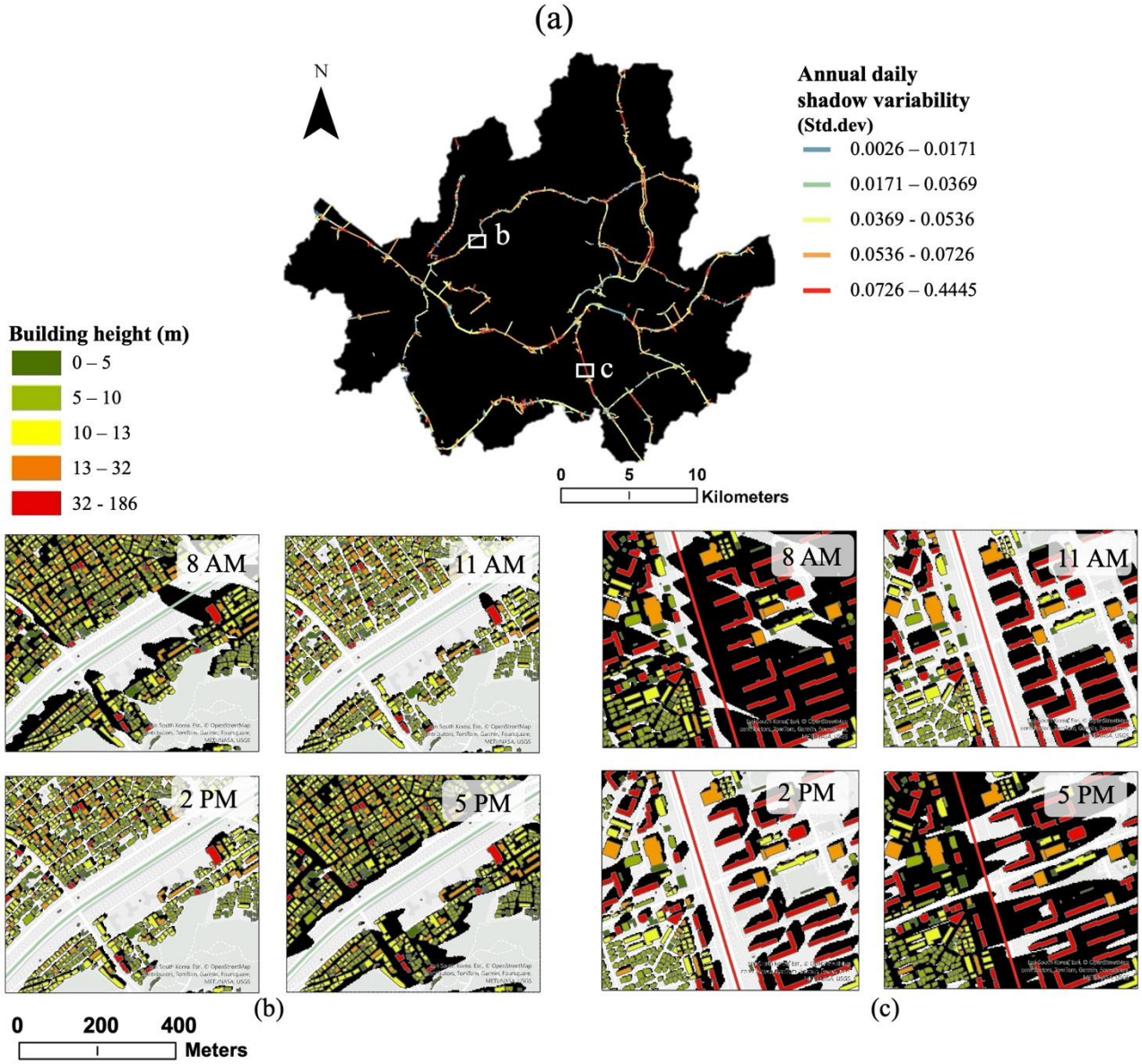

Figure 5. Spatial distribution of annual daily shadow variability: (a) Annual daily shadow variability on high-traffic roads, (b) Road belonging to a cluster with low shadow presence and low variability, (c) Road belonging to a cluster with high shadow presence and high variability.

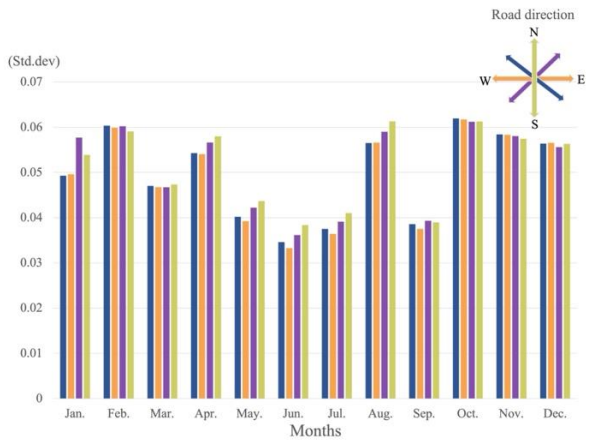

Figure 6. Monthly distribution of daily shadow variability by road direction clusters.

5. Conclusions

This research provides critical insights into temporal and spatial shadow variability, which have significant implications for urban planning, especially in the context of the impending commercialisation of SPVs. By combining a database of shadow measurements developed through this research with real-time weather data, it will be possible to precisely predict the solar power generation of SPV in urban area. This predictive capability can enhance route planning for SPVs by recommending paths that optimise solar energy generation based on time-specific and date-specific production variations.

The analysis reveals that shadow variability is profoundly influenced by seasonal changes and can also be affected by the directional orientation of roads. This highlights the crucial interplay between sun positioning and urban architectural dynamics, stressing the importance of managing sun exposure and shadows effectively in urban design. Such considerations are

vital for optimising the urban environment for both comfort and energy efficiency, particularly for the functioning of SPVs.

The use of spatial GIS analysis in this study emphasises its importance in enhancing the accuracy and understanding of urban shadow. By leveraging GIS, planners and designers can visualise the impacts of urban form on sunlight accessibility and shadow casting in different time scenarios. This is particularly important in narrow urban spaces, such as alleys, where buildings are closely spaced. Although this study focused primarily on high-traffic roads, the implications for narrower streets, often shadowed by both buildings and vegetation, are significant.

Further studies should consider the effects of tree shadows, which vary seasonally. Trees, closer to roads than buildings in many cases, cast extensive shadows in summer due to foliage but less so in winter when the leaves fall. This dynamic aspect of urban vegetation plays a critical role in the spatial and temporal patterns of shadow casting, thus affecting solar energy generation. Future research could also incorporate Light Detection And Ranging (LiDAR) scans to obtain higher-resolution DEM. The current DEMs used in this study have a resolution limit of 30 m due to civilian restrictions in South Korea (MOLIT, 2017). LiDAR technology could overcome these limitations by providing more detailed elevations, including those of trees, enhancing the precision of shadow and solar access calculations.

By addressing these elements, urban planners can better harness GIS tools to adapt city layouts for the optimal use of solar energy, thereby enhancing the performance of energy-efficient SPVs in urban environments.

Acknowledgements

This research was financially supported by the (1) Institute for Peace and Unification Studies (IPUS) at Seoul National University under the project of “Laying the Groundwork for Unification and Peace” and (2) was supported by a grant from the Human Resources Development program (No. 20204010600250) of the Korea Institute of Energy Technology Evaluation and Planning (KETEP), funded by the Ministry of Trade, Industry, and Energy of the Korean Government.

References

Bieker, G., 2021: A global comparison of the life-cycle greenhouse gas emissions of combustion engine and electric passenger cars. *Communications*, 49, 847129-847102.

Chalkias, C., Faka, A., Kalogeropoulos, K., 2013: Assessment of the direct sunlight on rural road network through solar radiation analysis using GIS. *Open J. Appl. Sci.*, 3, 224. doi.org/10.4236/ojapps.2013.32030.

Esri, 2023: ArcGIS Pro, How Hillshade works. Available online: https://pro.arcgis.com/en/pro-app/latest/tool-reference/3d-analyst/how-hillshade-works.htm (accessed on 18 August 2023).

Fan, Z., Fu, Y., Liang, H., Gao, R., Liu, S., 2023: A module-level charging optimization method of lithium-ion battery considering temperature gradient effect of liquid cooling and charging time. *Energy*, 265, 126331.

IEA (International Energy Agency), 2023: Transport. Available online: https://www.iea.org/energy-system/transport (accessed on 12 April 2023).

Kim, H.; Ku, J.; Kim, S.M.; Park, H.D., 2022: A new GIS-based algorithm to estimate photovoltaic potential of solar train: Case study in Gyeongbu line, Korea. *Renew. Energy*, 190, 713–729. doi.org/10.1016/j.renene.2022.03.130.

Ministry of Land, Infrastructure and Transport (MOLIT), 2017: National spatial information security management regulations Directive No. 949.

Ministry of Land, Infrastructure and Transport (MOLIT), 2021: Building information. Available online: http://www.molit.go.kr/portal.do (accessed on 4 February 2021).

NGII (National Geographic Information Institute), 2023: Centerline of road. Available online: http://ngii.go.kr/kor/main.do (accessed on 21 March 2023).

Oh, M.; Kim, S.M.; Park, H.D., 2020: Estimation of photovoltaic potential of solar bus in an urban area: case study in Gwanak, Seoul, Korea. *Renew. Energy*, 160, 1335-1348. doi.org/10.1016/j.renene.2020.07.048.

Rossi, R.; Ceccato, R.; Gastaldi, M., 2020: Effect of road traffic on air pollution. Experimental evidence from COVID-19 lockdown. *Sustainability*, 12(21), 8984. doi.org/10.3390/su12218984.

Senol, M.; Bayram, I. S.; Naderi, Y.; Galloway, S., 2023: Electric Vehicles Under Low Temperatures: A Review on Battery Performance, Charging Needs, and Power Grid Impacts. *IEEE Access*, 11, 39879-39912. doi.org/10.1109/ACCESS.2023.3268615.

The Ministry of Economy, Trade, and Industry (METI) and Space Administration (NASA), 2023: ASTER GDEM 003. Available online: https://asterweb.jpl.nasa.gov/gdem.asp (accessed on 7 May 2023).

Transportation Operation & Information Service, 2023: Traffic volume survey data in Seoul. Seoul Metropolitan Government. Available online: https://topis.seoul.go.kr/refRoom/openRefRoom_2.do (accessed on 7 May 2024).

Yoo, S. H., 2011: Simulation for an optimal application of BIPV through parameter variation. *Solar Energy*, 85(7), 1291-1301. doi.org/10.1016/j.solener.2011.03.022.